Frequency Invariant Classification of Ultrasonic Weld Inspection Signals

Robi Polikar, *Student Member, IEEE*, Lalita Udpa, *Senior Member, IEEE*, Satish S. Udpa, *Senior Member, IEEE*, and Tom Taylor

Abstract—**Automated signal classification systems are finding increasing use in many applications for the analysis and interpretation of large volumes of signals. Such systems show consistency of response and help reduce the effect of variabilities associated with human interpretation. This paper deals with the analysis of ultrasonic NDE signals obtained during weld inspection of piping in boiling water reactors. The overall approach consists of three major steps, namely, frequency invariance, multiresolution analysis, and neural network classification. The data are first preprocessed whereby signals obtained using different transducer center frequencies are transformed to an equivalent reference frequency signal. Discriminatory features are then extracted using a multiresolution analysis technique, namely, the discrete wavelet transform (DWT). The compact feature vector obtained using wavelet analysis is classified using a multilayer perceptron neural network.**

Two different databases containing weld inspection signals have been used to test the performance of the neural network. Initial results obtained using this approach demonstrate the effectiveness of the frequency invariance processing technique and the DWT analysis method employed for feature extraction.

I. Introduction

Ultrasonic methods of nondestructive testing are used extensively in the weld inspection of boiling water reactor piping for detecting intergranular stress corrosion cracking (IGSCC) [1]. IGSCC occurs in the heat-affected zone (HAZ) of welds in stainless steel piping. Three major factors that cause IGSCC to form and propagate are: tensile stresses on the inner diameter of the weld region, a corrosive environment, and a sensitized grain structure. The detection of IGSCC in the HAZ of welds in piping is of considerable interest to the nuclear industry.

IGSCCs are most often detected using an angle beam ultrasonic inspection method. This method involves launching an ultrasonic wave into the weld region, and analyzing the signal reflected back from a discontinuity present within the material. A schematic of the weld geometry is in Fig. 1. It can be seen that the received signal may be reflected from a crack, a counterbore, or a rootweld. The superposition of reflections from rootwelds and counterbores on the crack signals makes the interpretation of the resulting ultrasonic inspection signals very challenging.

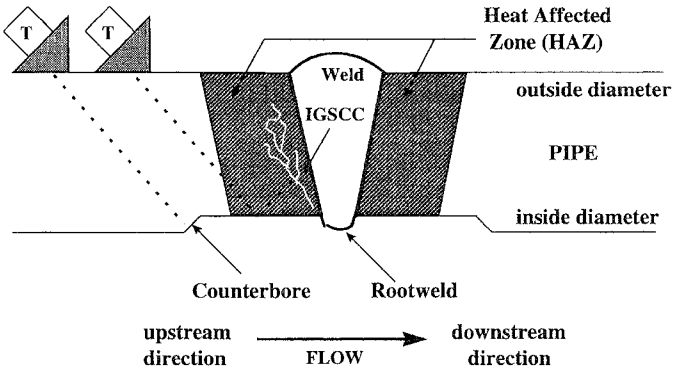

Fig. 1. Typical weld geometry for ultrasonic inspection.

Studies have shown that manual ultrasonic inspection can be accurate but is highly variable, depending on the inspection skills, training and emotional status or fatigue of inspectors [2], [3]. Automated signal classification (ASC) is becoming increasingly popular in many commercial applications, including nondestructive evaluation (NDE). Motivation for the use of such systems arises from the need for accurate interpretation of large volumes of inspection data, and minimizing errors due to human factors. ASC systems have the potential for detecting flaws and interpreting ultrasonic signals consistently and accurately. Such systems have the added advantage of being able to provide a quantitative measure of the probability of detecting flaws.

Pioneering work on automated ultrasonic data analysis dates back to the late 70s and early 80s when Rose and his colleagues [4], [5] reported promising results on the feasibility of using pattern recognition techniques for automatic characterization of signals using a set of features chosen from the spatial, frequency, and time domains. Other researchers have investigated the feasibility of using physical features from time and frequency representations of signals for flaw characterization. These include such features as maximum amplitude of the signal, pulse duration, waveform kurtosis, rise and fall times [6], [7].

Once a set of optimum features has been chosen, a suitable classifier can be used to classify the waveforms. A number of supervised and unsupervised classification algorithms such as K-means clustering algorithm, fuzzy C-means, and more recently neural networks have been proposed for classifying signals. Using a suitable training al-

Manuscript received March 14, 1997; accepted October 17, 1997. This work was supported by Electric Power Research Institute (EPRI) under contract RP3148-06. Project manager, J. Spanner.

R. Polikar, L. Udpa, and S. S. Udpa are with the Department of Electrical and Computer Engineering, Iowa State University, Ames, IA 50011.

T. Taylor is with Batelle Pacific Northwest Laboratories, Richland, WA 99352.

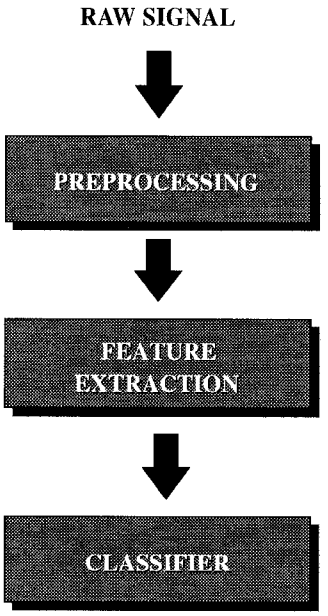

Fig. 2. Overall schematic of an automated signal classification system.

gorithm, these networks can be trained to learn the correlation between features in signals and the type of reflector. Neural networks have been used extensively in flaw characterization during the last decade, largely due to their ability to generate complex decision boundaries in the multidimensional feature space [8].

One of the issues of concern in piping weld inspection is that inspections may be conducted at different frequencies, depending on the needs of the problem at hand. Although the reflections at different frequencies contain different information, the objective of the signal classification system developed in this study was simply to classify the received signal as flaw or nonflaw in such a manner that the interpretation is insensitive to the transducer frequency. For the purposes of this study, defect sizing, and therefore the size of the flaw, was not an issue of concern.

Following a brief description of the overall approach in Section IIA, a detailed discussion of the method for accomplishing frequency invariance is given in Section IIB. The discrete wavelet transform feature extraction scheme and the neural network algorithm used for classification are presented in Sections IIC and IID, respectively. Two different databases of ultrasonic weld inspection signals that are used to evaluate the performance of the overall signal classification scheme are introduced in Section III. Results obtained are presented and discussed in Section IV, followed by concluding remarks in Section V.

II. Method

A. Overall Approach

The overall approach used for the ASC system consists of three major steps as shown in Fig. 2. In the preprocessing stage, the primary objective is to render the classification results invariant to the effects of variations in test and sample conditions including gain and frequency settings, time delays in sampled signals, and other minor differences in material properties. In this specific case, we are interested in developing a signal classification system such that the performance is reasonably insensitive to the choice of the transducer center frequency. This is accomplished using time scaling.

The second step involves the extraction of features to reduce the dimensionality of the signal to be processed by minimizing redundancy. The feature extraction algorithm employs the discrete wavelet transform (DWT). The frequency invariant signals obtained from the first stage are analyzed using DWT for extracting features containing sufficient discriminatory information.

The wavelet transform based features incorporating both time and frequency domain information are then classified using a neural network into one of three groups, namely, crack, counterbore, and rootweld. Each of the three steps are described in the following sections.

B. Preprocessing for Frequency Invariance: Time Scaling

In ultrasonic inspection, transducers of different center frequencies are used, depending on a number of issues, such as wall thickness, resolution desired, and the depth and the orientation of the flaw. Lower frequencies are used when the thickness of the sample is large enough for signal attenuation to be an important factor. However, high frequency transducers are used to resolve smaller flaws and for flaw sizing particularly when the thickness of the sample is small enough to allow attenuation issues to be ignored.

This poses a major problem when the data is analyzed using an ASC system. Most pattern classification algorithms rely heavily on the shape of the signal, which can vary considerably with the frequency of operation. Therefore, it is required that the ASC system recognize signals of different frequencies and interpret them in such a manner that the overall performance is independent of the frequency of operation. The frequency invariance technique described in this paper transforms signals at different frequencies to a reference frequency signal prior to feature extraction.

Fig. 3 shows two signals obtained from a crack using a 1 MHz transducer [Fig. 3(a)], and a 2.25 MHz transducer [Fig. 3(b)]. Figs. 4(a) and (b) show the frequency spectra of these two signals centered at 1 MHz and 2.25 MHz, respectively. If an ASC system is trained exclusively with 1 MHz signals, the higher frequency signal has to be transformed appropriately prior to classification.

A simple approach for frequency invariance is based on time-scaling that transforms both the center frequency as well as the bandwidth of the signal. Time scaling relies on simply scaling the time axis of a signal, resulting in either stretching or compressing the signal. Scaling in time

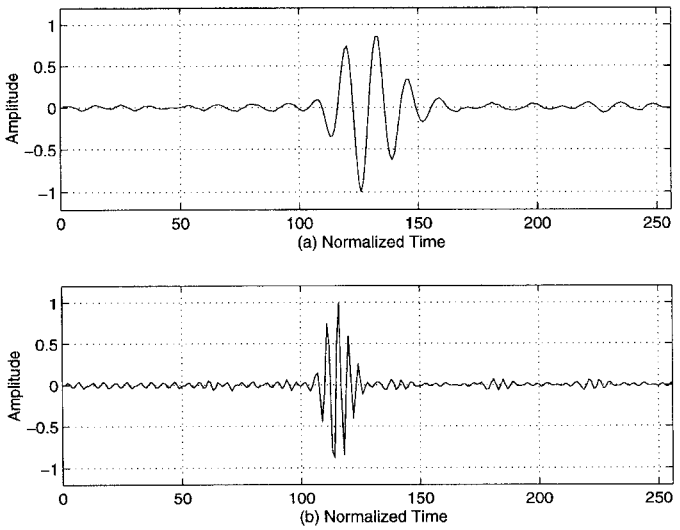

Fig. 3. Typical ultrasonic signals at 1 and 2.25 MHz.

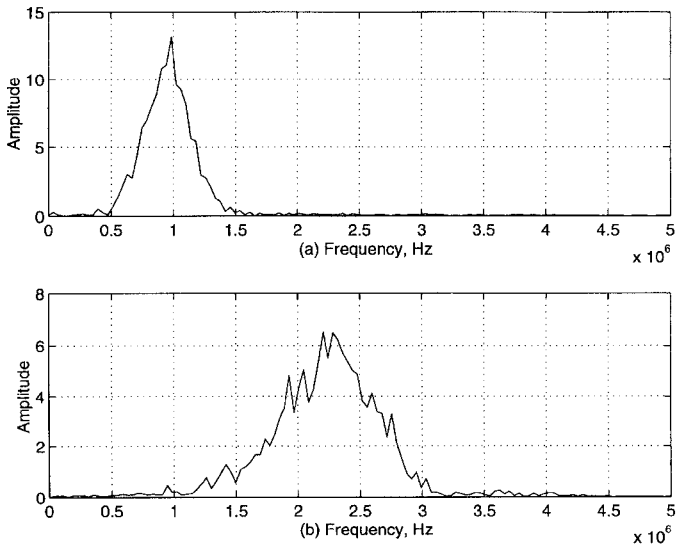

Fig. 4. Frequency spectrums of the sample signals at (a) 1 MHz, (b) 2.25 MHz.

domain is accomplished by using decimation and interpolation procedures as explained below.

A signal centered at frequency f_1 with bandwidth BW_1 is scaled in time so that its center frequency and bandwidth are mapped to f_2 and BW_2, respectively. This transformation of frequency f_1 to a frequency $f_2 = \frac{f_1}{a}$, exploits the FT property:

$$x(at) \Longleftrightarrow \frac{1}{a} X\left(\frac{f}{a}\right) \tag{1}$$

where $x(t) \Longleftrightarrow X(f)$.

Depending on the value of a, the transformed signal is either stretched or compressed in time. The time scaling is accomplished by a combination of interpolation and decimation operations. Decimating a signal by a factor of m involves dropping every mth sample whereas interpolating by a factor of m involves adding m new samples of appropriate amplitudes between each sample of the original signal. For example, the 2.25 MHz signal is scaled down in frequency to a 1 MHz signal by using $a = 2.25$, that is, the signal is interpolated by a factor of 9 and decimated by a factor of 4 to give a scaling factor of 2.25. The resulting 1 MHz signal has 2.25 times the original number of sample points. The number of points is then reduced to the original value by eliminating the samples at the two ends. This truncation is performed on the assumption that the discarded samples from each end of the interpolated signal do not carry any significant amount of information.

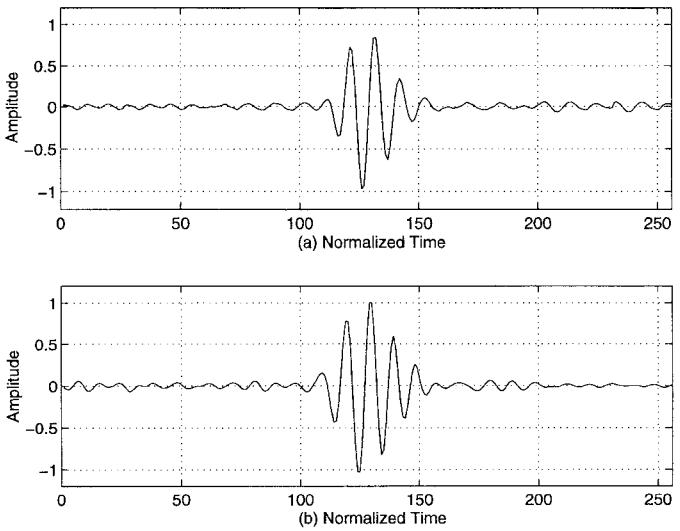

Fig. 5. (a) 1 MHz signal in time domain, (b) time scaled 2.25 MHz signal in time domain.

The time scaling procedure was implemented on the 2.25 MHz signals, a typical example of which is shown in Fig. 3(b). It can be seen that the first and last 64 samples of the 256 samples long sequence do not carry any significant information, and the bulk of the energy is concentrated in the midsection of the A-scan. Therefore, no information is lost by the truncation. Fig. 5 illustrates the 1 MHz signal and the time scaled version of the 2.25 MHz signal shown in Fig. 3(b). Fig. 6 shows the corresponding frequency spectra.

As seen in Fig. 6, both signals are centered at 1 MHz frequency, and their bandwidths are very similar. It is also seen that the overall shape of the spectrum has not been altered. In other words, all information has been retained during the time-scaling operation. The signals acquired at different inspection frequencies are transformed to the reference frequency of 1 MHz prior to feature extraction.

C. Feature Extraction: The Wavelet Transform

Ultrasonic NDE signals contain reflections from discontinuities which manifest in the A-scans as abrupt time localized changes resulting in time varying spectral characteristics. Consequently, the conventional Fourier decomposition technique is not an appropriate tool for analyzing these signals. The discrete wavelet transform is a mul-

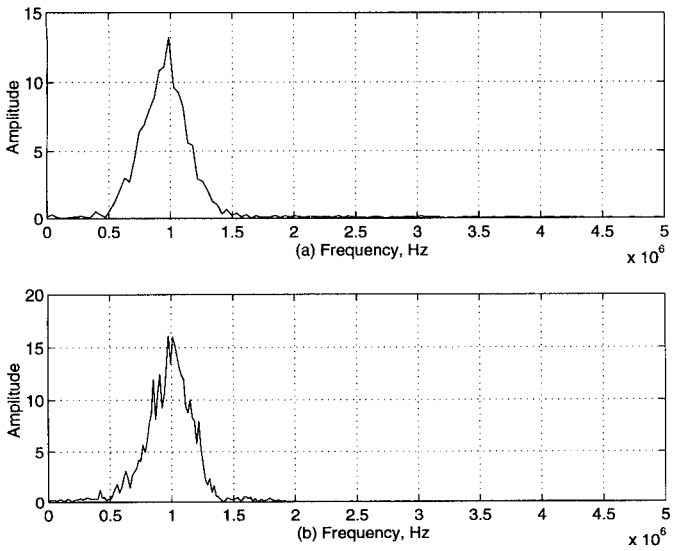

Fig. 6. (a) Frequency spectrum of the 1 MHz signal in Fig. 5(a), (b) frequency spectrum of the 2.25 MHz signal in Fig. 5(b).

tiresolution analysis technique which is one of several approaches that can be used to obtain the time-frequency representation (TFR) of a signal. The TFRs are used to analyze time localized signals with time-varying spectra, where conventional Fourier transform analysis methods prove to be inadequate.

Several methods have been used to obtain the TFR of signals with time varying spectra, such as short time Fourier transform (STFT) or Wigner distribution (WD). The constant time and frequency resolutions associated with the STFT and the inherent difficulty in the implementation of the WD on nonanalytical signals have limited the wide spread use of these methods. These limitations have been overcome by wavelet transforms, introduced to the signal processing community by Mallat [9] in the mid and late 1980s.

The (continuous) wavelet transform is defined as follows:

$$WT_x^{\psi}(\tau, s) = \Psi_x^{\psi}(\tau, s) = \frac{1}{\sqrt{|s|}} \int x(t)\psi^* \left(\frac{t-\tau}{s} \right) dt \tag{2}$$

where the transformed signal $WT_x^{\psi}(\tau, s)$ is a function of two variables, τ and s, representing translation and scale parameters, respectively, and $\psi(t)$ is the transforming function called the mother wavelet. The wavelet transform represents the correlation between the signal $x(t)$ and scaled versions of a prototype function, the mother wavelet. The scaling of the prototype function involves contraction and dilation of the signal, and the translation involves shifting this function along the time axis.

The discrete wavelet transform is a fast algorithm that is used to obtain the wavelet transform of a discrete time signal.

An extensive discussion of the discrete wavelet transform and theory of multiresolution analysis can be found in [10], [11]. The analysis technique discussed in this paper employs subband coding for representing ultrasonic signals, and this method will be described in greater detail.

The DWT analyzes the signal by decomposing it into its coarse approximation and detail information. This decomposition is accomplished by using successive highpass and lowpass filtering operations in the frequency domain.

The original signal $x[n]$ is first passed through a half-band highpass filter $g[n]$ and a lowpass filter $h[n]$, where $g[n]$ and $h[n]$ are quadrature mirror filters (QMF) of each other. Various filters have been developed over the years to be used in DWT computation, and among them Daubechies wavelets have found widespread use. After the filtering, half of the samples of the two output signals are discarded by subsampling, because the signals now have a bandwidth of $\pi/2$ radians instead of π. This constitutes one level of decomposition and is expressed mathematically as:

$$y_{\text{high}}[k] = \sum_n x[n].g[2k-n] \tag{3}$$

$$y_{\text{low}}[k] = \sum_n x[n].h[2k-n] \tag{4}$$

where $y_{\text{high}}[k]$ and $y_{\text{low}}[k]$ are the outputs of the highpass and lowpass filters, respectively, after subsampling by 2.

This decomposition in effect halves the time resolution and doubles the frequency resolution, because the frequency band of the signal now spans only half the previous frequency band. The above procedure is repeated for further decomposition of the lowpass filtered signals. The highpass filtered signals constitute the DWT coefficients. At every level, the filtering and subsampling results in half the number of samples spanning half the frequency band resulting in reduced time and improved frequency resolutions. Fig. 7 illustrates this procedure, where $x[n]$ is the original signal to be decomposed, and $h[n]$ and $g[n]$ represent lowpass and highpass filters, respectively. The bandwidth of the signal at every level is indicated by f in Fig. 7. This procedure in effect resolves the high frequencies better in time and the low frequencies better in frequency. Because most signals of practical interest are nonstationary in nature, subband coding provides a very effective way of obtaining the TFR.

The DWT coefficients at different levels are concatenated, starting with the last level (coarsest) coefficients. For a signal consisting of 256 samples, the first level (highest resolution) contains 128 samples, the second level contains 64, the third level contains 32, and so on. This algorithm provides an efficient decomposition if the number of samples is a power of two, or a multiple of power of 2.

DWT also provides a very effective signal compression and data reduction scheme. Because the energies of most signals are concentrated in a certain frequency band, all other frequencies are represented by very low amplitudes in the transform domain, and can be discarded without any loss of information. Figs. 8(a) and (b) show a typical ultrasonic 1 MHz crack signal sampled at 10 MHz and

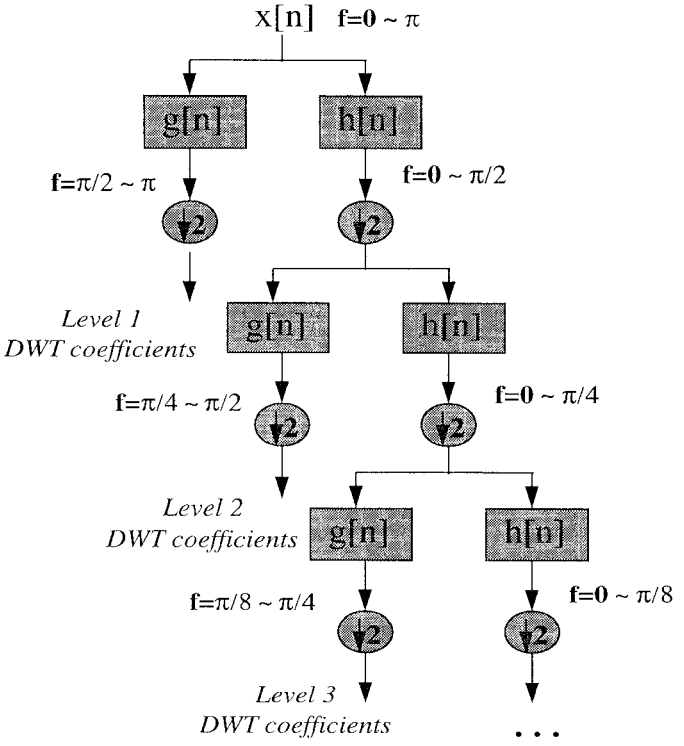

Fig. 7. Subband coding scheme for computing the DWT.

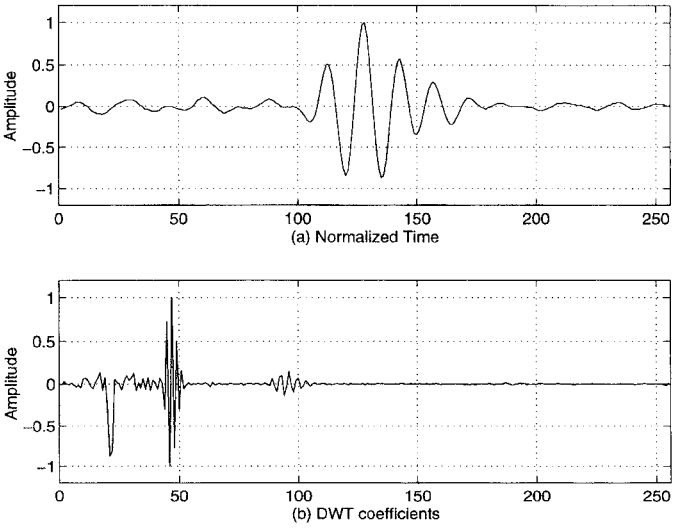

Fig. 8. A typical crack signal (a), and its DWT (b).

its DWT, respectively. The last 128 samples constituting Level 1 DWT coefficients (samples 129 through 256) characterize the signal in the $[\pi/2, \pi]$ rad/s frequency band, which corresponds to frequency range of 2.5 to 5 MHz. These samples do not carry much information, because the signal does not have any spectral components in this frequency range. Level 2 DWT coefficients (samples 65 through 128) characterize the signal in the $[\pi/4, \pi/2]$ rad/s frequency band corresponding to the frequencies 1.25 to 2.5 MHz. The main energy of the signal appears in the Level 3 DWT coefficients (samples 33 through 64), which characterize the signal in the $[\pi/8, \pi/4]$ rad/s range, corresponding to frequency range of 625 kHz to 1.25 MHz. The relatively large negative peak appearing in the Level 4 DWT coefficients, samples 16 through 32, correspond to the lower frequencies in the signal, including the envelope of the signal.

It can be easily seen that the 256 samples long signal can be represented by the first 128 samples of the DWT with little error, because the contribution of the last 128 coefficients is negligible. Therefore, the Level 1 DWT coefficients can be discarded without any loss of information. In this respect, DWT not only provides a feature extraction scheme, but also provides significant data reduction, thereby reducing the computational burden considerably. Because samples that are excluded are most likely to correspond to noise, this data reduction also improves the classification accuracy.

D. Neural Network Classification

A number of supervised and unsupervised pattern recognition algorithms have been employed for the classification of multidimensional signals. The K-means clustering algorithm is one of the most widely used techniques for partitioning the feature space. More recently neural networks have proved to be very effective in signal classification, due to their ability to generate arbitrarily complex decision boundaries [12].

A variety of neural network architectures and learning algorithms have been developed over the years, including the Hopfield, multilayer perceptron (MLP), radial basis functions, Kohonen, and adaptive resonance networks [13]. For classification of signals that are separated by complex decision boundaries in the feature space, the MLP networks have gained widespread acceptance and become the network of choice, due to their simple yet powerful learning algorithm.

In this application, we use the MLP for classifying the signals obtained from weld inspection into three classes, namely crack, counterbore, and rootweld. The network was trained using the well-known backpropagation algorithm [13]. Fig. 9 illustrates the architecture of the two-hidden layer MLP network used in this study, where I_i, $i = 1, 2, ..., N$ is the input vector, $H1_j$, $j = 1, 2, ..., N1$ are the output values of the first hidden layer nodes, $H2_k$, $k = 1, 2, ..., N2$ are the output values of the second hidden layer nodes, and O_l, $l = 1, 2, 3$ are the values at the output nodes.

The feature vector consists of 128 DWT coefficients requiring 128 input nodes. Two hidden layers with 30 nodes in the first hidden layer, 7 nodes in the second hidden layer, and an output layer with 3 nodes were used. The output layer was designed to generate binary valued signals. If the signal presented to the input node is a crack signal, the desired output is [1 0 0], whereas counterbore and rootweld signals produce outputs [0 1 0] and [0 0 1], respectively.

The weights connecting the input nodes to the first hidden layer nodes are denoted by u_{ij}, the weights connecting the first hidden layer nodes to the second hidden layer

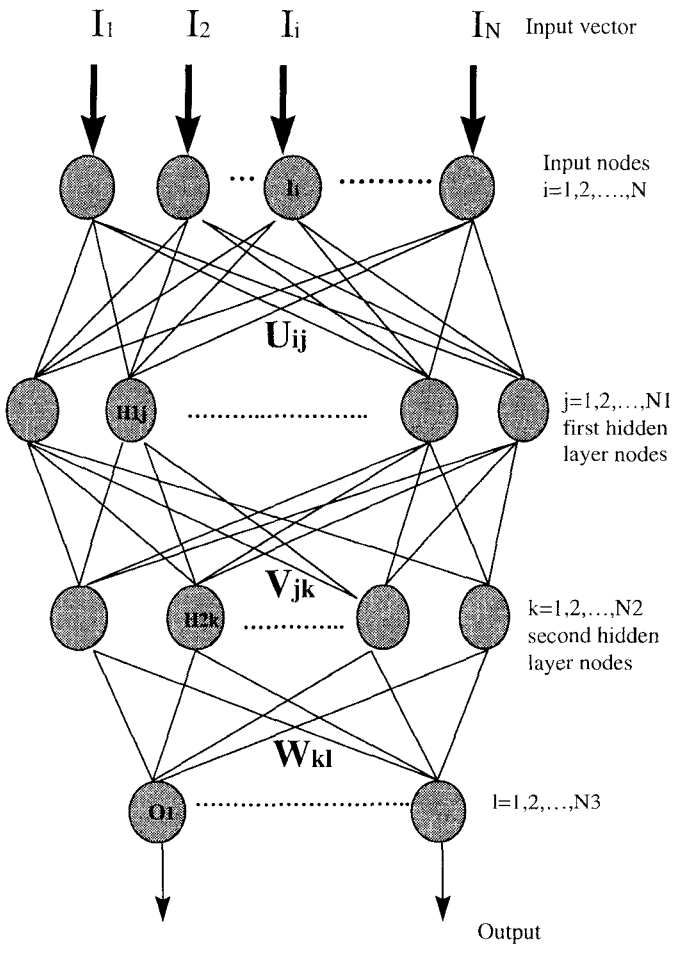

Fig. 9. Network architecture, the multilayer perceptron with two hidden layers.

nodes are denoted by v_{jk}, and finally the weights connecting the second hidden layer nodes to the output nodes are denoted by w_{kl}.

Additional nodes were added to both input and hidden layers with a constant value of 1 to serve as threshold levels in the network equations. These nodes always have the same state, 1, and do not change throughout the training process.

The input signal (vector) $\mathbf{I} = I_1, I_2, I_3, \ldots, I_N$, is fed to the input layer of the network which does not perform any computation. The values of the hidden layer nodes and the output nodes are computed as follows:

$$H1_j = f\left(u_{0j} + \sum_{i=1}^{N} u_{ij}.I_i\right) \quad j = 1, 2, \ldots, N1 \tag{5}$$

$$H2_k = f\left(v_{0k} + \sum_{j=1}^{N1} v_{jk}.H1_j\right) \quad k = 1, 2, \ldots, N2 \tag{6}$$

$$O_l = f\left(w_{0l} + \sum_{k=1}^{N2} w_{kl}.H2_k\right) \quad l = 1, 2, 3. \tag{7}$$

The activation function, f, used in the above equations is the sigmoid function defined by (8):

$$f(x) = \frac{1}{1 + e^{-\zeta.x}}. \tag{8}$$

The parameter ζ determines the slope of the sigmoid function; as ζ approaches infinity, the sigmoid function approaches a hard limiter function. The index 0 used in (5), (6), and (7) characterize the extra node added to introduce a threshold value.

Computing the output values of all nodes using the above equations constitutes a single forward pass. The training procedure is a recursive algorithm that starts at the output node and proceeds back to the first hidden layer (hence backpropagation). The weights are adjusted such that the error in the network output is minimized. The minimization is performed using a conventional gradient descent algorithm as explained in [13].

The convergence time of the network (the training time) can be reduced significantly with the right choice of the learning rate, η, which controls the rate at which the weights are adjusted in the gradient descent algorithm. Unfortunately, a well defined set of criteria for choosing the learning rate is not available. Choosing η too small increases the learning time considerably, whereas choosing a large value for η may cause the network to jump over or miss, the error surface minimum.

An alternate approach is to use an adaptive learning rate. In this method, the learning rate is constantly changed according to the change in the error from one iteration to the next. If the new error is greater than a predefined ratio α (typically 1.04) times the previous error, the new weights, output values, and errors are discarded, and the learning rate is decreased by a predefined factor β (typically 0.7). The learning then continues with the previous weights, error values, and node values. If the new error is less than the predefined ratio times the previous error, the learning rate is increased, again by a predefined factor γ (typically 1.2) [14].

The MLP parameters used in this study are summarized in Table I.

TABLE I
MLP/BP PARAMETERS.

Parameter	Value
Error goal	0.05
Initial learning rate	0.0001
α	1.04
β	0.7
γ	1.2
Momentum term	0.95
Number of input nodes	128
Number of hidden layers	2
Number of first hidden layer nodes	30
Number of second hidden layer nodes	7
Number of output nodes	3
Activation function	sigmoid

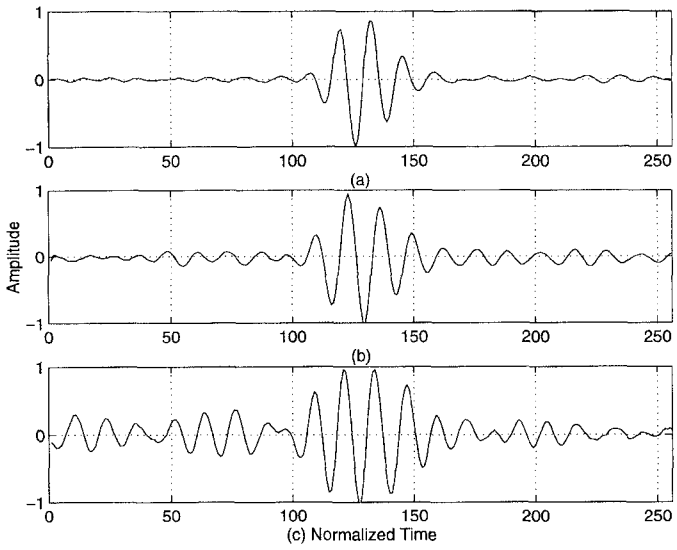

Fig. 10. Typical examples of each class: (a) crack, (b) counterbore, (c) rootweld.

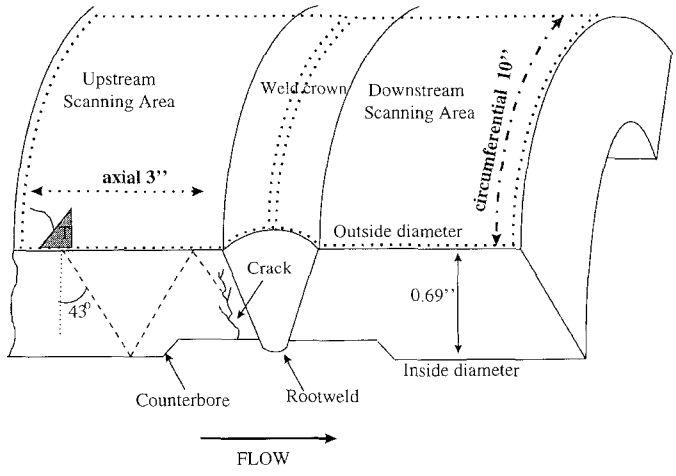

Fig. 11. The pipe geometry and the setup for the LMT database.

III. The Database and Implementation

Two databases containing weld inspection signals from nuclear power plant piping were used to evaluate the effectiveness of the approach. The data included three classes of signals, labeled as crack, counterbore, and rootwelds. Typical signals obtained from a crack, counterbore, and rootweld are illustrated in Fig. 10. A brief description of the two databases are given in the following subsections.

A. The EPRI Database

The first database considered was that generated by the Electric Power Research Institute (EPRI) IGSCC database and consisted of 539 controlled signals of known classification at 1 and 2.25 MHz frequencies. The conditions employed for generating this database can be found in [15]. The signals were single A-scans, 256 samples long, acquired at a sampling rate of 10 MHz. All signals were first individually normalized to a maximum amplitude of 1 in order to minimize the impact of the pulser receiver gain setting. A set of 160 signals of 1 MHz chosen at random from this database were used for training the network. The training dataset included 60 crack signals, 50 counterbore signals, and 50 rootweld signals. The DWT coefficients of these 160 signals were then computed using the Daubechies wavelets with four vanishing moments. The filter coefficients of Daubechies wavelets can be found in [16]. The first 128 of these coefficients were used to train the MLP.

B. The LMT Database

The second database, generated using an automated scanning system by Lambert, McGill, Thomas, Inc. (LMT), consisted of 32 C-scan images of 16 piping weld regions at 1 and 2.25 MHz. Each C-scan covers a scanning area of 3 in. in the axial direction and 10 in. in the circumferential direction. The A-scans were collected in steps of 0.025 in. in the axial direction and 0.1 in. in the circumferential direction, giving a total of $121 * 101 = 12{,}221$ A-scan signals per C-scan image. Each A-scan signal was sampled at 25 MHz to generate 1798 samples per signal. The C-scans were obtained by raster scanning the pipe either in the upstream direction (against the direction of the flow) or in the downstream direction (in the direction of flow). Fig. 11 illustrates the schematic of the inspection geometry used in generating the database.

In addition to the crack, counterbore, and rootweld signals, this database also included background signals. These signals were very easy to distinguish from others due to their low amplitude. All signals in this database were consequently thresholded to eliminate the background signals from further processing.

The remaining signals, each of length 1798, were then segmented using a 256 long window such that the maximum amplitude of the reflected waveform appears in the middle of the time window. The time window of interest for this gating and aligning process was computed based on the values of wall thickness, angle of incidence, propagation velocity, and transducer position relative to the weld. These signals were individually normalized in amplitude to a maximum of 1. The DWT coefficients of normalized signals were computed using the Daubechies wavelets with four vanishing moments, and the first 128 coefficients were used to train the network. The steps involved in the testing stage are summarized in Fig. 12.

A set of 125 signals of known classification were selected from the 1 MHz C-scan image shown in Fig. 13, containing all three classes of signals. These signals were equally distributed among the three classes: 42 signals from crack, 43 signals from counterbore, and 40 signals from rootweld regions. The neural network was trained using the 1 MHz A-scans. The test data included signals from all 32 C-scan images obtained using both 1 and 2.25 MHz transducers. During the testing stage, all 2.25 MHz signals were time-scaled before time aligning.

TABLE II
DISTRIBUTION OF SIGNALS IN THE EPRI IGSCC DATABASE.

Frequency	# of crack signals	# of counterbore signals	# of rootweld signals
1 MHz	98	73	75
2.25 MHz	107	94	92

TABLE III
PERFORMANCE OF THE NEURAL NETWORK DEMONSTRATING THE EFFECT OF TIME-SCALING AND DWT.

	Correct Classification (%)				
	DWT			FFT	
	Column 1	Column 2	Column 3	Column 4	Column 5
Class	1 MHz	unscaled 2.25 MHz	scaled 2.25 MHz	1 MHz	scaled 2.25 MHz
Crack	96%	34%	93%	84%	76%
Counterbore	100%	20%	97%	86%	67%
Rootweld	95%	61%	96%	87%	95%

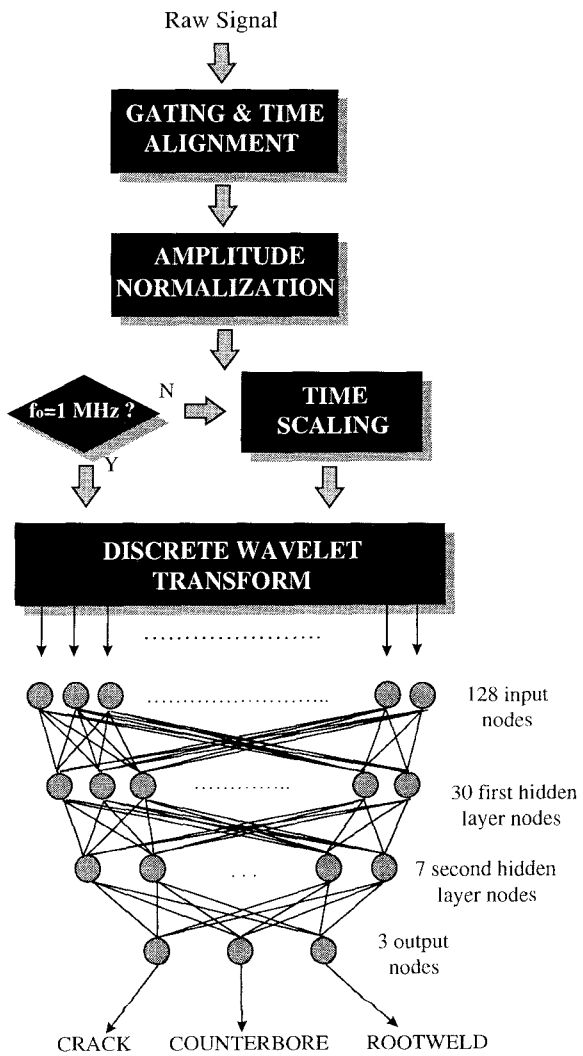

Fig. 12. Overall procedure.

IV. RESULTS AND DISCUSSION

The performance of the ASC system was tested on two different sets of data, namely, the EPRI IGSCC database and the LMT database. The results are presented and discussed in the following subsections.

A. Results Using the EPRI Database

Test signals from the EPRI database consisting of individual A-scans at frequencies of 1 and 2.25 MHz were distributed into three classes as shown in Table II.

Three different tests were performed to evaluate the overall approach in general, and the time scaling and the discrete wavelet transform processing techniques in particular. The results are summarized in Table III.

In test I, the MLP was trained with 1 MHz signals and tested with 1 MHz signals. The network performed very well as seen in Column 1 of Table III by correctly classifying 96% of the cracks, 100% of the counterbores, and 95% of rootwelds.

In test II, the same network was tested with the raw, unscaled 2.25 MHz signals. The network performed very poorly as seen in Column 2 of Table III, classifying only 34%, 20%, and 61% of the crack, counterbore, and rootweld signals, respectively.

In test III, the same network trained with 1 MHz signals, was tested with the time-scaled 2.25 MHz signals. The classification performance improved significantly as seen in Column 3 of Table III. The network correctly classified 93% of the cracks, 97% of the counterbores, and 96% of the rootwelds.

Signals from each class vary significantly, depending on the frequency of operation. Training the network with both 1 and 2.25 MHz signals within the same training data either prevents the network from converging or causes it to perform very poorly due to these large variations within individual classes at different frequencies. The results of

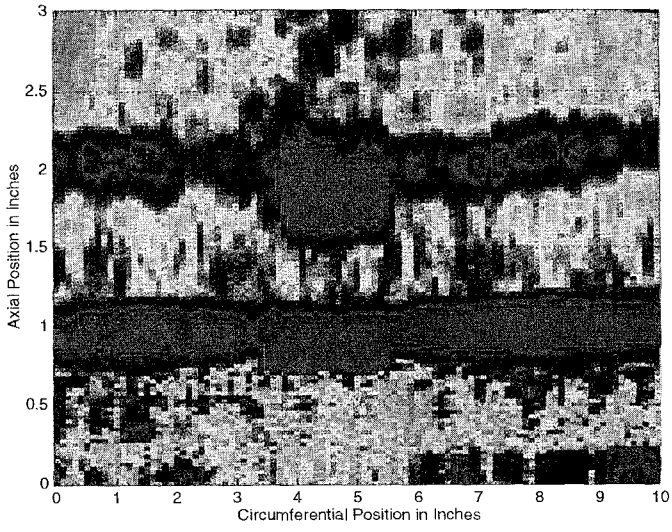

Fig. 13. Typical C-scan image.

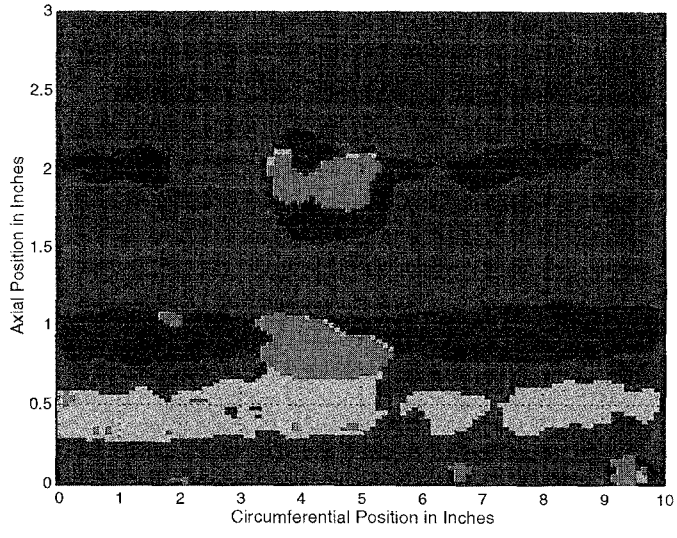

Fig. 14. Neural network generated version of the C-scan in Fig. 13: red, crack; cyan, counterbore; yellow, rootweld; blue, background.

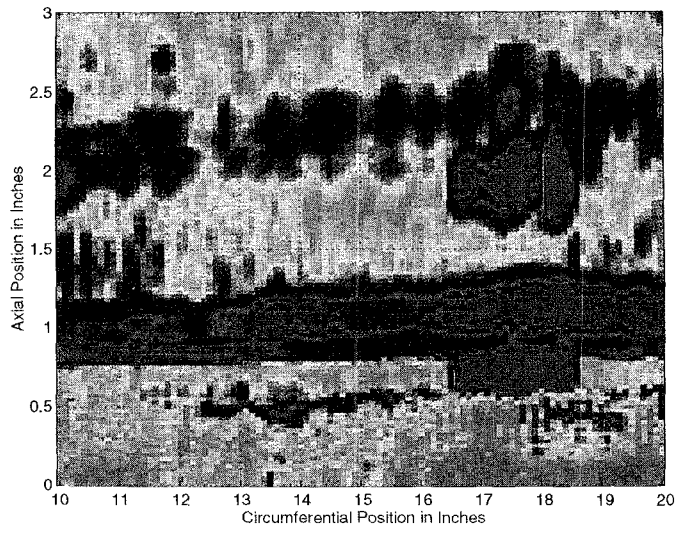

Fig. 15. A 2.25 MHz C-scan image.

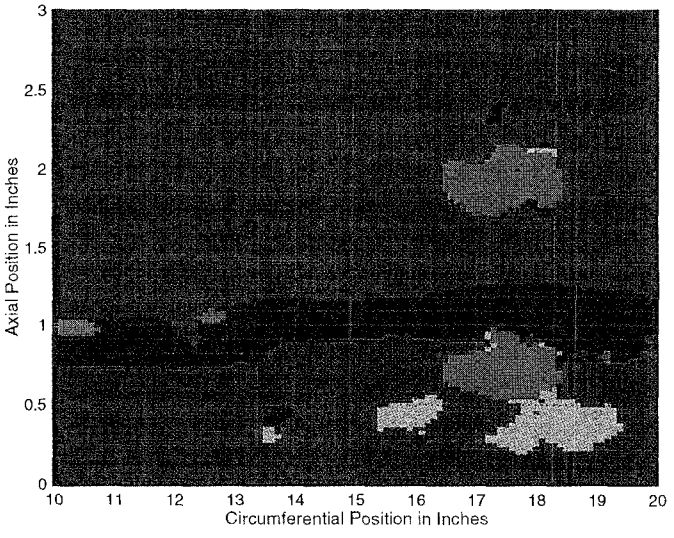

Fig. 16. Neural network generated version of the C-scan in Fig. 15: red, crack; cyan, counterbore; yellow, rootweld; blue, background.

these tests illustrate the effectiveness of the time scaling procedure in removing the frequency-dependent variations while retaining the discriminatory features of different classes.

In order to evaluate the choice of the DWT coefficients as elements of the feature vector, the performance was assessed using feature vectors containing 128 fast Fourier transform (FFT) coefficients. The network was trained with 1 MHz signals, and tested with the remaining 1 MHz signals and time-scaled 2.25 MHz signals. These results are illustrated in Columns 4 and 5 of Table III. The classification performance with FFT coefficients supports our initial arguments describing the need for using nonstationary signal processing techniques such as the DWT for analyzing ultrasonic signals.

The performance of the neural network classification was compared with that obtained using conventional clustering techniques such as the K-means clustering algorithm. The feature vector containing 128 DWT coefficients obtained as before was input to the K-means clustering algorithm. The entire EPRI database, including 1 MHz and time-scaled 2.25 MHz signals, was used. The performance of the clustering algorithm was significantly poorer than that of the neural network. All cracks were correctly classified, but only 43% of the counterbores and 45% of the rootwelds were detected. All misclassified counterbores and rootwelds were labeled as cracks, resulting in a significant number of false alarms.

The K-means clustering algorithm is a very simple scheme that performs well with lower dimensional feature vectors. However, in the case of complex feature spaces, neural networks have shown superior classification performance [17]. In addition, the K-means clustering algorithm suffers from other drawbacks, such as sensitivity of the performance to the choice of initial cluster centers and the order in which the data is presented.

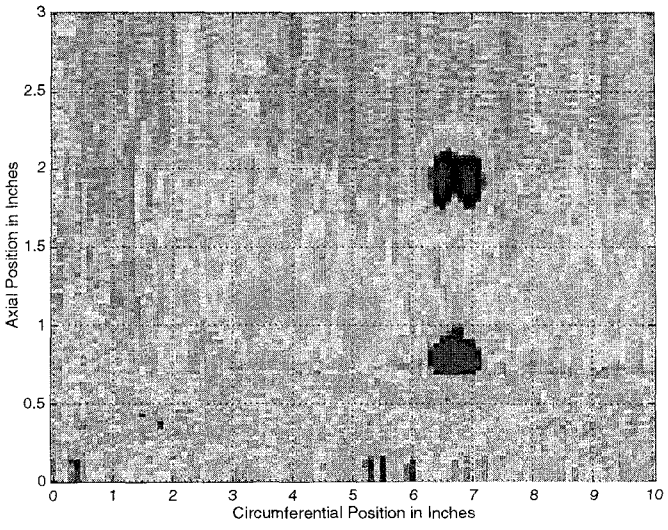

Fig. 17. A 1 MHz C-scan image with crack indications only.

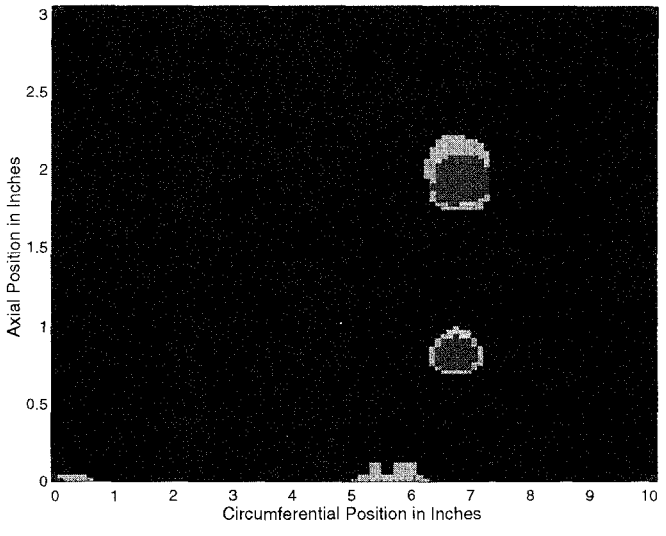

Fig. 18. Neural network generated version of the C-scan in Fig. 17: red, crack; cyan, counterbore; yellow, rootweld; blue, background.

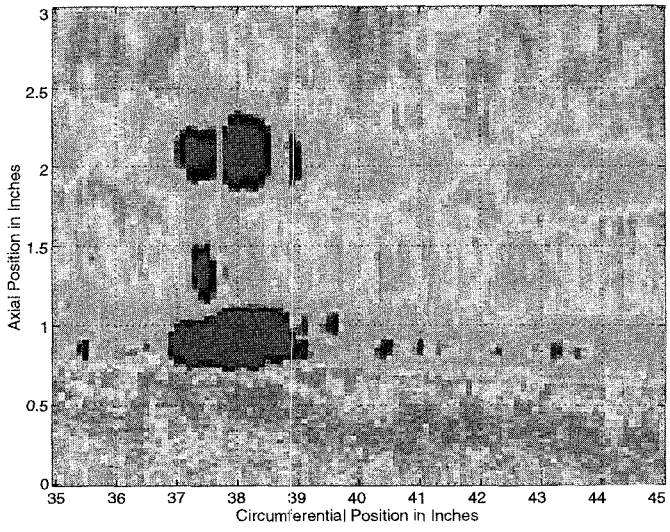

Fig. 19. A 2.25 MHz C-scan image with crack indications only.

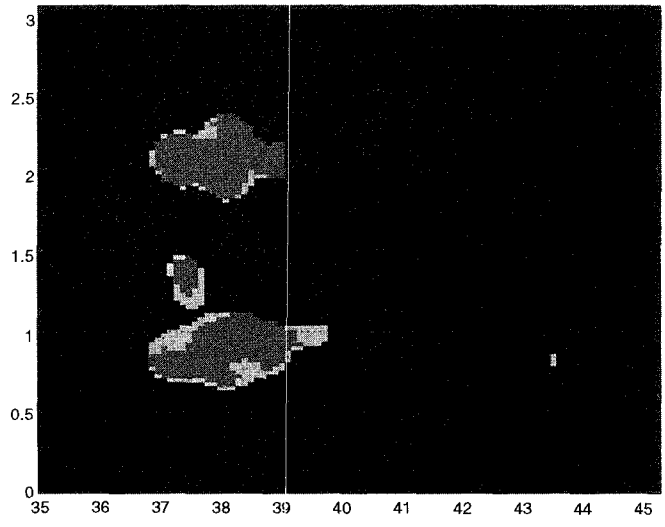

Fig. 20. Neural network generated version of the C-scan in Fig. 19: red, crack; cyan, counterbore; yellow, rootweld; blue, background.

It is apparent from Table III that the performance of the neural network is optimized when time scaling is employed and DWT coefficients are used as features.

B. Results Using the LMT Database

The ASC system was then applied to the C-scan images in the LMT database. The results of the neural network classification are presented as "neural network generated images" of the corresponding C-scans. A typical example of a C-scan image indicating regions of cracks, counterbores, and rootwelds used in this study is shown in Fig. 13. As mentioned earlier, the signals used to train the neural network were randomly selected from this C-scan image.

The horizontal and vertical axes correspond to the circumferential and axial positions of the transducer on the pipe, respectively. Each point on the C-scan reflects the maximum amplitude in the time windowed A-scan at the corresponding transducer position. The red stripe that runs along the axial position 1 in. represents a counterbore region, except that the midsection corresponding to circumferential positions ranging from 4 to 6 in., which represents a region with a crack. Corresponding indications due to the second reflection are seen in the axial positions from 1.7 to 2 in. The second irregular strip along the axial position of 0.5 in. represents a rootweld region.

The neural network generated classification image is shown in Fig. 14. Cracks in the resulting image are represented in red, counterbores in green, rootwelds in yellow, and background signals are represented in blue. The neural network clearly identified all crack, counterbore, and rootweld regions correctly as seen in Fig. 14.

The neural network was then tested on a 2.25 MHz C-scan image. The raw C-scan and the corresponding classification images are presented in Figs. 15 and 16. The crack is located at the axial position of 0.7 in. and circumferential position between 16.5 and 18.5 in. The irregular strip

across the image at the axial position of 1 in. represents a counterbore. The region that covers the axial positions of 0.3 to 0.5in. and the circumferential positions of 17.5 to 19.5in. represents a rootweld region. Fig. 16 shows the neural network classification of the crack, counterbore, and rootweld regions at the appropriate locations.

Fig. 17 shows a C-scan representing data acquired using a 1 MHz transducer from a specimen with two regions of interest corresponding to a crack and its second reflection. The neural network classification is shown in Fig. 18. Except for a few isolated misclassified pixels, the neural network generated image clearly depicts the crack regions. Simple image processing techniques, such as median filtering, can be used to post process the classification image to eliminate isolated pixels being classified as counterbores or rootwelds.

Fig. 19 illustrates another C-scan obtained from a region with crack indications. This C-scan also was generated using a 2.25 MHz transducer. The neural network generated image is shown in Fig. 20. As seen from Fig. 20, the neural network clearly indicated the crack regions.

Most of the 32 C-scan images contained only cracks with no counterbore or rootweld indications, similar to the C-scan images shown in Figs. 17 and 19. All the IGSCC indications were successfully identified by the neural network. Four images presented in this section are representative of the entire database.

V. Conclusions

The results obtained demonstrate the validity of the overall strategy that employs time scaling for invariance to the effect of transducer frequency, the wavelet transform for feature extraction, and neural networks for classification. Time scaling is a simple operation for transforming signals of the same class obtained at different excitation frequencies to a single reference frequency signal so that a single neural network can perform the classification independent of the transducer frequency. This procedure can be used safely when the indications of defect are present at both frequencies, and when defect detection, rather than defect sizing, is the primary objective. The discrete wavelet transform was chosen for feature extraction largely due to the fact that time and frequency information are provided simultaneously for time localized signals, and significant data reduction is obtained without major loss of information.

Neural networks trained using a specific set of weld inspection data may not perform well if there are significant changes in pipe geometries and material properties. A certain amount of retraining is inevitable under such situations.

Several issues are still being investigated. One effort that is in progress is to predict the confidence level of the network performance. The ASC system developed in this study is currently being enhanced to include features that allow the network to predict the reliability of its own classification. Variations in pipe geometries and material properties may be reflected in the confidence level of the network prediction, which in turn will determine the need for further training.

In an attempt to demonstrate the versatility of the approach developed, the automated signal classification system is currently being evaluated to test the robustness using different databases and crack morphologies. Future plans include participation in the Performance Demonstration Initiative (PDI) organized by EPRI to test Level 3 ultrasonic inspectors for certification.

References

[1] R. Thompson and D. Thompson, "Ultrasonics in nondestructive evaluation," *Proc. IEEE*, vol. 73, pp. 1716–1755, Dec. 1985.

[2] P. Heasler, T. Taylor, J. Spanner, S. Doctor, and J. Deffenbaugh, *Ultrasonic Inspection Reliability for Intergranular Stress Corrosion Cracks.* Report, NUREG/CR-4908, May 1990.

[3] J. Spanner, R. Badalamente, W. Rankin, and T. Triggs, *Human Reliability Impact on Inservice Inspection.* Report, NUREG/CR-4436, Mar. 1986.

[4] J. Rose and G. Singh, "A pattern recognition reflector classification study in the ultrasonic inspection of stainless steel pipe welds," *Br. J. Non-Destr. Test.*, vol. 21, pp. 308–311, Nov. 1979.

[5] J. Rose, M. Avioli, and M. Lapides, "A physically modeled feature based ultrasonic system for IGSCC classification," *Mater. Eval.*, vol. 40, no. 13, pp. 1367–1383, Dec. 1982.

[6] T. Case and R. Waag, "Flaw identification from time and frequency features of ultrasonic waveforms," *IEEE Trans. Ultrason., Ferroelect., Freq. Contr.*, vol. 43, pp. 592–600, July 1996.

[7] S. Burch, "A physical approach to the automated ultrasonic characterization of buried weld defects in ferritic steel," *NDT Int.*, vol. 19, pp. 145–153, June 1986.

[8] A. Masnata and M. Sunseri, "Neural network classification of flaws detected by ultrasonic means," *NDT&E Int.*, vol. 29, pp. 87–93, 1996.

[9] S. Mallat, "A theory for multiresolution signal decomposition: the wavelet representation," *IEEE Trans. Pattern Anal. Machine Intell.*, vol. 11, pp. 674–693, July 1989.

[10] O. Rioul, "A discrete time multiresolution theory," *IEEE Trans. Signal Processing*, vol. 41, pp. 2591–2606, Aug. 1993.

[11] A. Akansu and R. Haddad, *Multiresolution Signal Decomposition: Transforms, Subbands, and Wavelets.* San Diego CA: Academic, 1992.

[12] R. Lippmann, "An introduction to computing with neural nets," *IEEE ASSP Magazine*, vol. 4, pp. 4–22, Apr. 1987

[13] S. Haykin, *Neural Networks, A Comprehensive Foundation.* New York: Macmillan College Publ. Co., 1994.

[14] H. Demunt and M. Beale, *Neural Network Toolbox for Use with MATLAB.* Natick, MA: Math Works, 1992.

[15] Electric Power Research Institute, *RF Waveform Database for BWR IGSCC Ultrasonic Examination.* Revision 0, EPRI Report, 1989.

[16] I. Daubechies, "Orthonormal bases of compactly supported wavelets," *Commun. Pure Appl. Math.*, vol. 41, pp. 909–996, 1988.

[17] L. Udpa and S. S. Udpa, "Eddy current defect characterization using neural networks," *Mater. Eval.*, vol. 48, pp. 342–347, Mar. 1990.

Robi Polikar (SM'92) was born in Istanbul, Turkey, in 1972. He received his B.S. degree in electronics and communication engineering from Istanbul Technical University, Istanbul, Turkey, in 1993, and the M.S. degree in electrical engineering and biomedical engineering from Iowa State University, Ames, IA, in 1995. He currently is a Ph.D. student at Iowa State University in electrical engineering and biomedical engineering.

Mr. Polikar's research interests are in signal processing, neural network, and pattern recognition applications for biomedical engineering and nondestructive evaluation. He is a member of Tau Beta Pi, Eta Kappa Nu, and a student member of IEEE, as well as EMB, SP, and UFFC societies of IEEE.

Lalita Udpa (S'84–M'86–SM'91) received her Ph.D. in electrical engineering from Colorado State University in 1986. She currently is an associate professor of electrical engineering at Iowa State University, Ames, IA. Dr. Udpa works primarily in the area of nondestructive evaluation (NDE). Her research interests include numerical modeling of the forward problem and solution of the inverse problem in NDE. She works extensively on the application of signal processing, pattern recognition, and neural network algorithms for characterization of NDE signals. She is a senior member of IEEE, and a member of ASNT, Sigma Xi, and Eta Kappa Nu.

Satish S. Udpa (S'79–M'79–S'80–S'82–M'82–M'83–SM'91) received his M.S. and Ph.D. degrees in electrical engineering from Colorado State University in 1980 and 1983, respectively. Prior to that he received the B.Tech degree in electrical engineering from N.J.T. University, India, in 1975. He served as a faculty member at Colorado State University before joining Iowa State University, Ames, IA, in 1990. Currently, he is a professor in the Department of Electrical and Computer Engineering.

Dr. Udpa is involved with the development of signal processing and pattern recognition techniques for solving inverse problems relating to nondestructive testing. He also is engaged in the application of numerical techniques for modeling a wide variety of physical processes underlying nondestructive evaluation methods. He is a senior member of IEEE, and a member of ASNT, Phi Kappa Phi, and Eta Kappa Nu.

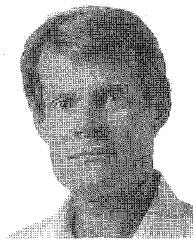

Tom Taylor has worked for more than 20 years in NDE research and has extensive experience in research project management. During the time frame of his work, he was the EPRI project manager.

Mr. Taylor has been active for more than 10 years on ASME Section XI Code and was a leading developer of the ultrasonic technology for the inspection of Hanford's N-reactor power tubes. His expertise covers the reactor pressure vessel, piping, balance of plant piping, and project management.